Arabian Journal of Chemistry (2020) 13, 4310–4323

King Saud University

Arabian Journal of Chemistry

www.ksu.edu.sa
www.sciencedirect.com

ORIGINAL ARTICLE

A mononuclear copper(II) complex containing benzimidazole and pyridyl ligands: Synthesis, characterization, and antiproliferative activity against human cancer cells

Sedat Kacar [a,*], **Hakan Unver** [b], **Varol Sahinturk** [a]

[a] *Department of Histology and Embryology, Faculty of Medicine, Eskisehir Osmangazi University, Eskisehir, Turkey*
[b] *Chemistry Department, Faculty of Science, Eskisehir Technical University, 26470 Eskisehir, Turkey*

Received 31 May 2019; accepted 13 August 2019
Available online 23 August 2019

KEYWORDS

Copper(II) complex;
MTT cytotoxicity;
Immunocytochemistry;
H-E;
DU145 human prostate cancer cells;
SPC mesothelioma cells;
NIH/3T3 fibroblast cells;
Apoptosis

Abstract Metal complexes are recently being hybridized with different moieties to discover new drugs due to their advantageous attributes. Among the metals, copper is a good one to synthesize a metal complex due to its being endogenous, redox and DNA cleavage potential, reported anticancer efficacies and selective permeability for cancer cells. In this study, first we synthesized a new copper (II) complex and determined its toxic doses on NIH/3T3 normal fibroblast cells, SPC212 mesothelioma and DU145 prostate cancer cells. Then, we ascertained anti-proliferative, apoptotic, morphological, oxidative and endoplasmic reticulum (ER) stress inducing effects of these newly synthesized compounds on DU145 prostate cancer cells. A novel Copper(II)/1-(4-(trifluoro methyl)benzyl)-1H-benzimidazole/2,2′-bipyridyl complex was synthesized and mainly characterized by single crystal X-ray diffraction analysis. Anti-proliferative effect of copper(II) complex was gauged by MTT. Oxidative and ER stress were evaluated by ELISA and Western blot. The morphological effect was examined by microscope analysis. Besides, immunocytochemistry of Bax, a pro-apoptotic protein and PCNA, a proliferation marker protein was performed. As a result, the inhibitory effect of newly synthesized substance was superior to the chemicals from which it was synthesized. Its IC_{50}s against DU145 were 37.0, 21.1 and 10.0 μM for 24, 48 and 72 h-treatments, respectively. Oxidative and ER stress increased after treatment. In microscopy, we observed apoptotic hallmarks like nuclear condensation, cellular shrinkage and membrane

* Corresponding author.
E-mail addresses: skacar@ogu.edu.tr (S. Kacar), hakanunver@eskisehir.edu.tr (H. Unver), varols@ogu.edu.tr (V. Sahinturk).
Peer review under responsibility of King Saud University.

Production and hosting by Elsevier

https://doi.org/10.1016/j.arabjc.2019.08.002

blebbings. In immunochemistry, increased Bax and decreased PCNA were apparent. Copper(II) complex with its relatively low IC_{50} can also be tested on other cancer and normal cell lines.

1. Introduction

Metal complexes are recently being investigated and combined with different moieties to discover new drugs since they have a couple of advantageous properties in terms of the number of coordination bounds they make, their flexible nature of geometries as well as their redox states (Qi et al., 2018). Furthermore, to hybridize the molecules with metals such as copper is a facile and affordable way to synthesize a chemical and presents numerous ways to make a new hybrid molecule. *Cis*-diamminedichloroplatinum, known as cisplatin, is also a metal complex of central platinum with 2 chloride and 2 ammonia molecules and broadly utilized in cancer treatment as a chemotherapeutic drug for years. However, it has several side effects, such as nephrotoxicity, hematologic toxicity and neurotoxicity (Florea and Büsselberg, 2011). Therefore, new drug candidates with low IC_{50} and fewer side effects are a matter of urgency.

Benzofuran—conjugated iridium complexes exert antiproliferative effects on DU145 prostate cancer cells *in vitro* and inhibit tumor growth *in vivo* by inhibiting STAT3 and NF-KB (Kang et al., 2017). These complexes also serve as an inhibitor of Ras/Raf-1 interaction, which takes role in tumor growth (Liu et al., 2017) as well as a luminescence probe for monitoring the ovarian carcinoma cells (Wang et al., 2017). Rhodium complexes selectively inhibit Lysine-Specific Demethylase 5, an overexpressed protein in breast cancer (Yang et al., 2018). Moreover, rhodium complexes target and kill the cells with DNA base mismatches (Boyle and Barton, 2018). Ruthenium complexes are utilized to target DNA and destruct it by photocytotoxicity (Burke et al., 2018). Among the metals, copper is a good one to synthesize a metal complex. First, it is an endogenous metal rather than an exogenous one like platinum and thus less toxic. Second, it has considerable redox and DNA cleavage potentials (Wang et al., 2015). Third, it is reported to be selectively permeable to membranes of cancer cells and their level is delicately regulated in cells (Apelgot et al., 1986). In addition, different copper complexes have been tried on various cancer cell line (Fan et al., 2010; Santini et al., 2014) and relatively low IC_{50} values are reported. Therefore, the copper complex proved to be highly effective against cancer cells. Thus, hybridizing the copper with different chemical moieties has the potential to pave the way for discovering new chemicals with strong anticancer activities.

Benzimidazole is the benzo derivative of imidazole. It is an indispensable part of many biologically crucial molecules, including vitamin B12. It has a number of biological activities, including, antimicrobial, antifungal, anticancer, antiviral, antifungal, antihypertensive, antihistaminic, anti-inflammatory, analgesic and anti-ulcer, etc. (Salahuddin and Mazumder, 2017). There are several studies pointing out the anti-cancer activity of benzimidazole derivatives. To mention some of them, novel Schiff base substituted benzimidazole derivatives exerted anti-proliferative effect on HeLa human cervical, MCF-7 breast, SW60 colon and MiaPaCa-2 pancreas cancer cell lines at micromolar levels (Hranjec et al., 2011). Gellis et al. examined the effect of several benzimidazole derivatives on T47D breast, A549 lung and HT29 colon cancer cells and discovered the anti-proliferative effect of them (Gellis et al., 2008). In another study, 2-substituted benzimidazole derivatives inhibited proliferation of HepG2 liver, MCF-7 and HCT 116 human cancer cell lines (Refaat, 2010). Besides, trisubstituted benzimidazole and its precursors were found to inhibit the proliferation of MDA-MB-231 human breast cancer cells (Thimmegowda et al., 2008). Also, copper complexes of benzimidazole documented by Zhao et al. exhibited inhibitory activity on SMMC7721-human liver, BGC823 human gastric, HCT116 human colon and HT29 human colorectal cancer cell lines (Ja et al., 2017).

Bipyridyl ligands have the potential to make two nitrogen coordination bounds in the copper complexes. Regarding pyridyl, in one study, most of the 24 hybrid 2-pyridyl- thiazole derivatives were found to have cytotoxic effect on HL-60 human leukemia, MCF-7, HepG2 and NCI-H292 lung cancer cell lines (dos Santos Silva et al., 2017). In another study, most of the 36 novel pyridyl-oxadiazole derivatives tested on MCF-7 exhibited considerably high cytotoxic activity (Khalil et al., 2015). In addition, a copper complex of pyridyl ligand was also reported to inhibit human cervical and breast cancer cell lines (Balakrishna et al., 2010).

Altogether, as above-mentioned reasons, we decided to synthesize a copper(II) complex with 2,2′-bipyridyl (bipy) and benzimidazole ligands $[Cu(CF)_2(bipy)(ClO_4)](ClO_4)$. In this study, first we determined toxic doses of this complex on NIH/3T3 normal fibroblast cells, SPC212 mesothelioma and DU145 prostate cancer cells and then we sought to ascertain anti-proliferative, apoptotic and morphological effects of these newly synthesized compound on DU145 prostate cancer cells.

2. Materials and methods

2.1. Materials-instrumentation-physical measurements

All of the reactants and solvents were obtained commercially (Sigma-Aldrich) at good quality and used throughout. The crystallographic measurements were performed with a Bruker AXS diffractometer. ^1H NMR experiment was performed using JEOL ECZ 500R. d^6-DMSO was used as solvent. Proton resonance frequency was adjusted to 500.13 MHz. Zerofilling was performed 1024 times, number of scans was adjusted as 128, and NMR spectra was obtained at 40 °C. The photoluminescence spectra for the copper complex were measured with a PerkinElmer LS 55 Fluorescence spectrometer. Elemental analysis was conducted with Elementar Vario EL III microanalyzer. FT-IR spectra were recorded with Perkin Elmer Spectrum 100 Spectrometer. Melting points were measured with a Stuart SMP-30 melting point apparatus.

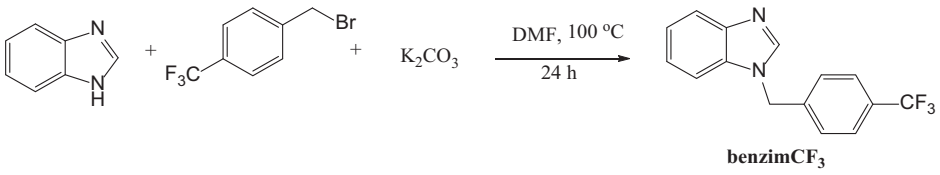

Fig. 1 The synthesis of the benzimCF_3 ligand.

2.2. Synthesis of the benzimidazole ligand, (benzimCF_3)

Ligand synthesis is depicted in Fig. 1. To a solution of 1H-benzimidazole (1 eq, 4.23 mmol, 500 mg) and potassium hydroxide (1.2 eq, 5.08 mmol, 285 mg) in 20 mL dimethyl sulfoxide, 10 mL dimethyl sulfoxide solution of trifluoromethylbenzyl bromide (0.8 eq, 3.38 mmol, 0.525 mL) was added drop by drop over 30 min. The resulting suspension was left to stir overnight at 80 °C. After the reaction was completed, the solution was cooled to room temperature and quenched with water. The precipitated product was extracted with diethyl ether three times and dried over magnesium sulfate. Evaporation of the solvent gave beige solid product after one day (Lygin and de Meijere, 2009) (877 mg; Yield: 75%; m. p.:75 °C) Anal. Calc. for $C_{15}H_{11}F_3N_2$ (276.26 g/mol) C,65.2; H,4.0; N,10.1. Found: C,65.3; H,4.1; N,10.2. FT-IR (KBr, ν cm^{-1}): 3084 υ(Ar—CH); 1617 υ(C═N); 1460 υ(C═C).

2.3. Synthesis of the copper(II) complex, [Cu(benzimCF_3)$_2$(bipy)(ClO_4)](ClO_4)

The synthesis procedure of copper(II) complex is given in Fig. 2. To a solution of copper(II) perchlorate hexahydrate (1 eq, 0.29 mmol, 107 mg) in 10 mL methanol, bipy solution (1 eq, 0.29 mmol, 45 mg) in 10 mL methanol was added dropwise and the solution was left to stir for 1 h at room temperature. After that, 10 mL methanolic solution of benzimidazole derivative (2 eq, 0.58 mmol, 160 mg) was added dropwise and the final dark blue solution was stirred for 12 h at 60 °C. The resulting solution was filtered over blue ribbon filter paper and X-ray suitable prismatic crystals were obtained by slow evaporation of the solvent after 5 days. (124 mg; Yield: 44%); Anal. Cal. for $C_{40}H_{30}Cl_2CuF_6N_6O_8$ (971.15 g/mol) C, 49.5; H, 3.1; N, 8.7%, Found: C, 49.6; H, 3.2; N, 8.6%. FT-IR (KBr, ν cm^{-1}): 3114 υ(Ar—CH); 1620 υ(C═N); 1520 υ(C═C); 622 υ(ClO_4). ^{1}H NMR (400 MHz, DMSO-d_6, δ ppm): 8.57 (s, 2H); 7.66 (s, 4H); 7.41 (s, 4H); 7.16 (s, 4H); 6.82 (d, 2H); 6.67 (s, 2H), 6.49 (s, 2H); 6.25 (s, 2H); 5.69 (s, 4H); 1.19 (s, 4H).

2.4. X-ray structure determination of copper(II) complex

Complex diffraction data were collected with Bruker AXS APEX-II CCD diffractometer equipped with a rotation anode at 296.15 K, respectively using graphite monochromated Mo Kα radiation at λ = 0.71073 Å. The data process was done with the Bruker SMART program package. **[SMART, Bruker AXS, (2000)]** Using Olex2, (Dolomanov et al., 2009) the structure was solved with the ShelXS (Sheldrick, 2008) structure solution program using Direct Methods and refined with the ShelXL (Sheldrick, 2015) refinement package using Least Squares minimization. The molecular structures were drawn at MERCURY (Macrae et al., 2008).

2.5. Cell culture and treatment

DU145 cells were cultivated in a high glucose Dulbecco's modified Eagle's medium, a commercial ready-to-use medium, containing fetal bovine serum and penicillin/streptomycin (10:1) at 37 °C in a CO_2 incubator. The cells reaching to 80–85% confluence were detached by 0.25% Trypsin-0.53 mM EDTA solution. 100 mM stock solution of copper(II) complex was carefully (A9099, Sigma-Aldrich, St. Louis, MO, USA) prepared in 1.5 mL tubes and at once stocked in aliquots in −20 °C until experiment day. Just before the experiment, one aliquot was melted, diluted in freshly prepared medium and immediately applied to the cells.

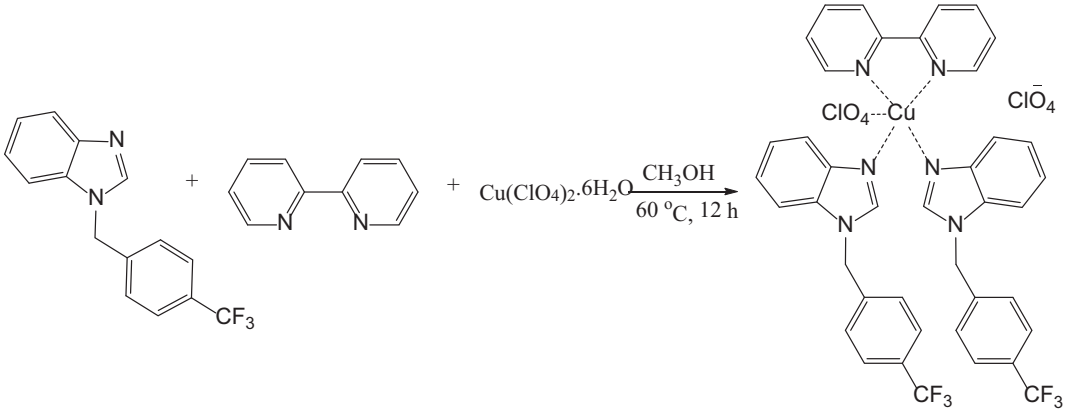

Fig. 2 Synthesis of the [Cu(benzimCF_3)$_2$(bipy)(ClO_4)](ClO_4) complex.

2.6. MTT assay

To gauge cellular viability, MTT (3-(4,5-dimethylthiazol-2-yl)-2,5-diphenyltetrazolium bromide) colorimetric assay was executed. In this assay, tetrazolium dye is reduced to solid formazan crystals through the activity of mitochondrial succinate dehydrogenase. The cells were cultured in 96-well plates at a density of 5×10^3 cells per well), and varying doses (0–200 μM) of a substituted benzimidazole, CF), a copper salt, copper (II) perchlorate hexahydrate with the formula of $Cu(ClO_4)_2{\cdot}6H_2O$ (CU), bipyridyl (bipy) and copper(II) complex were applied for 24, 48 or 72 h. Thereafter, the media were discarded, and the cells were incubated with freshly prepared 100 μL of MTT for 3 h. Next, solid formazan crystals were solubilized in 100 μL of DMSO at room temperature. In the end, the absorbance values were quantified at 570 nm by an ELISA reader (800TS, BioTek Instruments, Winooski, VT, US). The percentages of cellular viability were estimated with the formula below:

$$(\text{OD of the copper(II) complex-treated cells} - \text{OD of blank})/(\text{OD of control cells} - \text{OD of the blank}) \times 100,$$

where OD denotes optical density.

2.7. Oxidative status evaluation

DU45 cells were grown in 6-well plates and untreated or treated with three doses of copper(II) complex (25, 37 and 50 μM) in a total of 2 mL medium for 24 h. Then, adherent cells were washed delicately by ice-cold PBS (pH = 7), scraped by 500 μL of cold RIPA lysis buffer including protease inhibitor cocktail, (sc-24948, Santa Cruz Biotechnology, CA, USA) and collected in 1.5 mL tubes. The supernatant was discarded and the pellet was resuspended. Resuspended cells were vortexed intermittently for 30 min on ice. Thereafter, the cells were centrifuged at 16,000*g* for 10 min. Protein levels of the supernatant were determined by Qubit 2.0 Fluorometer by using the Qubit protein determination kit (Thermo Fisher Scientific, Waltham, Massachusetts, USA). Cell lysates for total antioxidant (TAS) and total oxidant status (TOS) were measured according to the commercial kits (Rel Assay Diagnostics, Gaziantep, Turkey), and oxidative stress status (OSI) was calculated by the following formula:

$$\text{OSI} = (\text{TOS}, \mu\text{mol } H_2O_2 \text{ Equiv./L.} / \text{TAS}, \mu\text{mol Trolox Equiv./L}) \times 100.$$

2.8. Western blot analysis

The cell lysates were also used for determination of endoplasmic reticulum (ER) stress via Western blot. Briefly, lysates were loaded onto gel as 50 μg per well. The samples were run in 7.5% (w/v) gel with colored ladder. After electrophoresis, the proteins were transferred to the PVDF membrane. Transferred membrane was blocked with 5% BSA, prepared in TBS-T, for 1 h at room temperature and incubated with mouse anti-GRP78 (sc-376768, Santa Cruz, USA) overnight +4 °C. Then, the membrane was incubated with the goat anti-mouse secondary antibody for one hour at room temperature. Finally, the image was developed as chemiluminescent by C-Digit device (Licor, Lincoln, US). The bands obtained from the western blot assay were analyzed using image J program.

2.9. Inverted microscope

DU45 cells were grown on coverslips in the twelve-well plate and untreated or treated with three doses of copper(II) complex (25, 37 and 50 μM) in a total of 2 mL medium for 24 h. Then, the plates were observed and photographed under an inverted microscope.

2.10. Hematoxylin-Eosin (H&E) staining

Hematoxylin and eosin (H-E) staining is one of the main and commonly utilized staining for years and demonstrates a wide range of extracellular matrix, cytoplasmic, nuclear properties of tissue and cells (Chan, 2014). In H-E, nucleus and cytoplasm stain as blue and pink, respectively. However, in some degenerative cases, staining can change and also form of a mixture of blue-pink colors. DU145 cells were cultivated in 6 well plates at a density of 5×10^5 cells per well. Then, the cells were untreated or treated with copper(II) complex for 24 h. Next, the cells were fixed with ice-cold methanol and stained with hematoxylin for 3 min and with eosin for 2 min. Finally, the cells were mounted onto a slide and examined under the light microscope.

2.11. May-Grunwald-Giemsa staining

In addition, a modified version of Clark's May-Grunwald-Giemsa staining was performed to examine the morphology of the cells (Clark, 1981). DU145 cells were cultivated in 6 well plates by being seeded at a density of 5×10^5 cells per well. Then, the cells were untreated or treated with copper(II) complex for 24 h. Next, the cells were fixed with ice-cold methanol and stained with May-Grunwald solution for 2 min and with Giemsa for 5 min. Finally, the cells were mounted onto a slide and examined under the light microscope.

2.12. Nuclear staining with DAPI

For nuclear details, DAPI staining was performed. DU145 cells were cultivated in 6 well plates at a density of 5×10^5 cells per well. Then, the cells were untreated or treated with copper (II) complex for 24 h. Next, the cells were fixed with ice-cold methanol and stained with DAPI for 15 min in darkness. Finally, the cells were mounted onto a slide and examined under the fluorescence microscope.

2.13. Immunocytochemistry (IM)

DU145 monolayer cells were plated at a density of 5×10^5 on six-well plates and treated with 25 and 37 μM of copper(II) complex for 24 h. Then, the cells were fixed with pure ice-cold methanol for a maximum of 10 min, ensuing 3 PBS washes. Later, the cells were blocked for 10 min, ensuing 3 PBS washes. Next, cells were incubated with primary antibodies against Bax (Santa Cruz Biotechnology, CA, USA) and PCNA (Bioss Antibodies Inc., MA, USA) overnight at 4 °C

by providing sufficient humidity. Afterward, the cells were incubated with biotinylated goat anti-polyvalent and streptavidin-peroxidase reagents (TP-125-HL, Thermo Scientific, US), respectively for 10 min each. Finally, the cells were mounted onto a slide and examined under the light microscope.

2.14. Statistics

Significance of MTT data was assessed by exploiting SPSS software (Statistics for Windows, Version 21.0. IBM Corp. Armonk, NY, USA). Entire data proved to be distributed normally by Kolmogorov-Smirnov test. Homogeneity of data was tested by Levene's test and all data were homogenous. Altogether, one-way analysis of variance (ANOVA) followed by post-hoc Tukey's test was applied. The mean + SD values of data were presented, and $p < 0.05$ was deemed statistically significant.

3. Results

3.1. X-ray analysis of the complex

The reaction between copper(II)perchlorate hexahydrate ($Cu(ClO_4)_2{\cdot}6H_2O$), 1-(4-(trifluoromethyl)benzyl)-1H-benzimidazole, *(benzimCF$_3$)* and 2,2′-bipyridyl successfully gave the new copper(II) complex $[Cu(benzimCF_3)_2(bipy)(ClO_4)](ClO_4)$. The complex crystal structure was mainly characterized by single crystal X-ray diffraction analysis and consistent with the FT-IR and Elemental Analysis values. The crystallographic data, refinement parameters, selected bond lengths and angles are given in Tables 1 and 2. The molecular structure of Cu(II) complex shown as ORTEP and ChemDraw are given in Fig. 3-4 with 30% thermal ellipsoid probability level.

Table 1 Crystal data and structure refinement for the complex.

Empirical formula	$C_{40}H_{30}Cl_2CuF_6N_6O_8$
Formula weight	971.14
Temperature	296.15 K
Wavelength	0.71073 Å
Crystal system, space group	triclinic, P-1
Unit cell dimensions	a = 12.6046(16) Å alpha = 95.786 (9) ° b = 13.1820(19) Å beta = 94.214 (8) ° c = 14.019(2) Å gamma = 114.495 (8) °
Volume	2091.6(5) A^3
Z, Calculated density	2, 1.542 Mg/m^3
Absorption coefficient	0.736 mm^{-1}
F(000)	986
Crystal size	0.12 × 0.11 × 0.08 mm
Theta range for data collection	2.944 to 57.206 deg.
Limiting indices	$-16\leq h\leq 16$, $-16\leq k\leq 17$, $-18\leq l\leq 18$
Reflections collected/unique	30783/10244 [R(int) = 0.0772]
Completeness to theta	28.603 95.6%
Absorption correction	Multi-Scan
Refinement method	Full-matrix least-squares on F^2
Data/restraints/parameters	10.244/0/568
Goodness-of-fit on F^2	1.097
Final R indices [I > 2sigma (I)]	R1 = 0.1045, wR2 = 0.2820
R indices (all data)	R1 = 0.1579, wR2 = 0.3306
Largest diff. peak and hole	1.91 and −1.18 $e.A^{-3}$

Table 2 Selected bond distances (Å) and bond angles and torsion angles (°).

Bond Distances (Å)	Bond Angles and Torsion Angles (°)
Cu(1)—N(1) 2.008(4)	N(1)—Cu(1)—N(2) 80.21(18)
Cu(1)—N(2) 2.020(4)	N(2)—Cu(1)—N(5) 92.56(18)
Cu(1)—N(3) 1.988(4)	N(5)—Cu(1)—N(3) 90.72(18)
Cu(1)—N(5) 1.982(4)	N(3)—Cu(1)—N(1) 94.10(17)
Cu(1)—O(3) 2.287(4)	

The complex crystallized in the triclinic P-1 space group. Copper(II) center is five coordinated by four nitrogen atoms (N1, N2, N3 and N5) of benzimCF$_3$ and bipy ligands and one oxygen atom (O3) of perchlorate anion, resulted in distorted square pyramidal geometry. The two bond distances between copper center and bipy ligand as Cu—N(1) and Cu—N(2) are identical and measured as 2.008 and 2.020 Å. Bond distances of Cu—N(3) and Cu—N(5) between benzimCF$_3$ ligands and copper center were found to be similar as 1.988 and 1.982 Å. In addition, the distance between anionic perchlorate oxygen and copper was found to be 2.287 Å. The bond angles of copper(II) complex and four nitrogen atoms vary between 80.21 and 94.10° and are nearly perpendicular to each other. All these data are in agreement with literature values (Kumar et al., 2019; Liu et al., 2018; Unver, 2018).

3.2. Spectroscopic study

Complex FT-IR spectrum was analyzed in the region of 400–4000 cm^{-1} and showed compatibility with single crystal X-ray structure. Peak observed at 1617 cm^{-1} in the uncoordinated benzimCF$_3$ ligand shifted to 1620 cm^{-1} after Cu—N coordination. The aromatic ring protons υ(Ar—CH) of both free benzimCF$_3$ and bipy ligands observed at 3084 cm^{-1}, appeared at 3114 cm^{-1} after the metal-ligand coordination. Additionally, perchlorate peak was observed at 622 cm^{-1} in the complex spectrum.

From the ^{1}H NMR spectrum of copper complex (Fig. S4), singlet peak observed at 1.19 ppm is related to methylene (—CH_2—) protons of benzimidazole ligand. Singlet and doublet signals around 7.16–7.66 ppm and 5.69 ppm are related to aromatic ring protons of benzimidazole ligand. In addition, signals observed between 6.25 and 6.82 ppm are dedicated to pyridyl ligand protons.

3.3. Cytotoxicity results

The cytotoxic effect of copper(II) complex on the proliferation of DU145 cells was quantified by the MTT colorimetric assay, as demonstrated in Figs. 5–9 and Tables 3 and 4. MTT assays of CF, CU, bipy and copper(II) complex were carried out at 3 different time intervals as 24, 48 and 72 h.

According to MTT results of CF, in the 24-hour treatment, at the doses lower than 200 μM, no significant decrease in cell

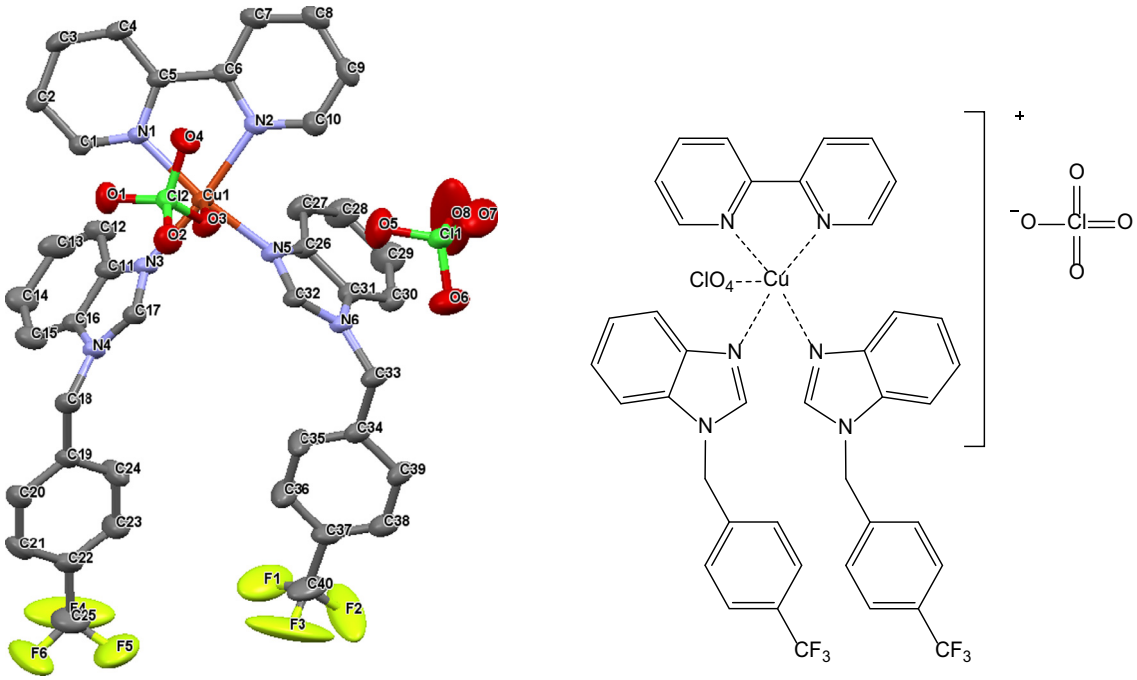

Fig. 3-4 [Cu(bipy)(benzimCF_3)$_2$(ClO_4)](ClO_4) complex molecular and ChemDraw structures with 30% thermal ellipsoid probability level (Hydrogen atoms were omitted for clarity).

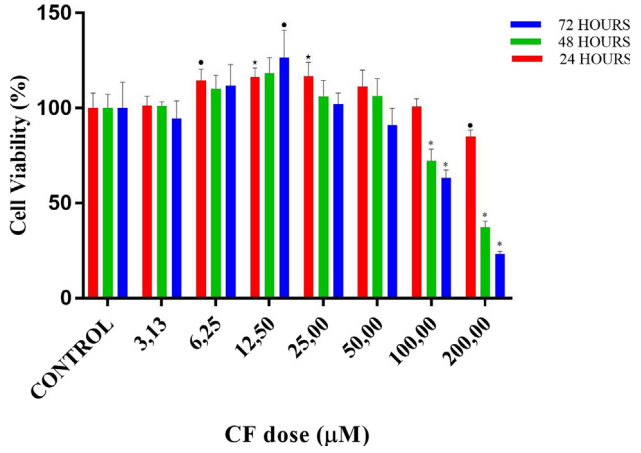

Fig. 5 Cell viability percentages vs different doses of fluorobenzimidazole derivative (CF) according to MTT assay results. •, ★ and * designate significant difference of $p < 0.05$, $p < 0.01$ and $p < 0.001$, respectively when compared to control.

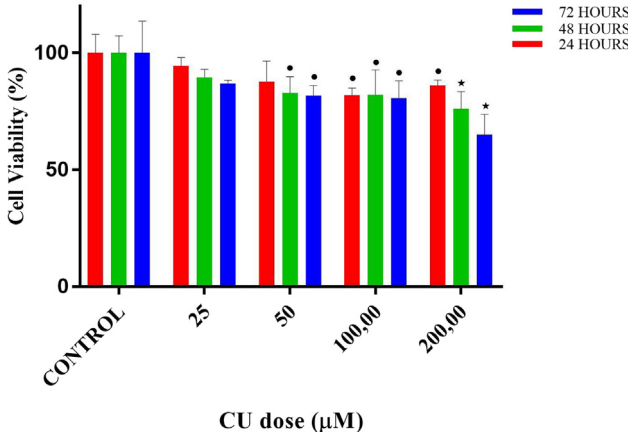

Fig. 6 Cell viability percentages vs different doses of 2. Copper II perchlorate hexahydrate (CU) according to MTT assay results. • and ★ designate significant difference of $p < 0.05$ and $p < 0.01$, respectively when compared to control.

viability was observed. On the contrary, at the doses of 6.25 ($p < 0.05$ vs control), 12.5 and 25 μM (both $p < 0.01$ vs control), significant proliferative activity was detected. At the highest applied dose, 200 μM cell viability lowered to around 85%. In the 48-hour treatment, no significant change in cell viability was observed until the dose of 100 μM, despite an upward trend of cell viability at the doses of 6.25 and 12.5 μM. On the other hand at the doses of 100 and 200 μM, cell viabilities lowered to 72.4 and 37.1%, respectively (both $p < 0.001$ vs control). In the 72-hour treatment, similarly, no significant decrease in cell viability was observed until the dose of 100 μM. However, there was a significant proliferative action at the dose of 12.50 μM ($p < 0.05$ vs control). On the other hand, at the doses of 100 and 200 μM, cell viabilities lowered to 63.3 and 23.3%, respectively (both $p < 0.001$ vs control).

According to MTT results of CU, in the 24-hour treatment, at the doses of 25 and 50 μM, no significant difference was detected when compared to control, despite downward trend (94.5 and 87.7%, respectively, both $p > 0.05$) in cell viability. However, at the doses of 100 and 200 μM, cell viabilities decreased to 81.8 and 86.1%, respectively ($p < 0.05$ vs control). In the 48-hour treatment, at the doses of 25, no significant difference was detected when compared to control,

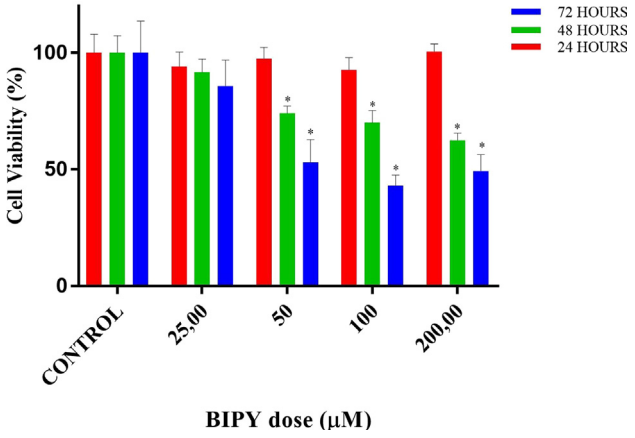

Fig. 7 Cell viability percentages vs different doses of bipyridyl (BIPY) according to MTT assay results. * designate significant difference of $p < 0.001$, respectively when compared to control.

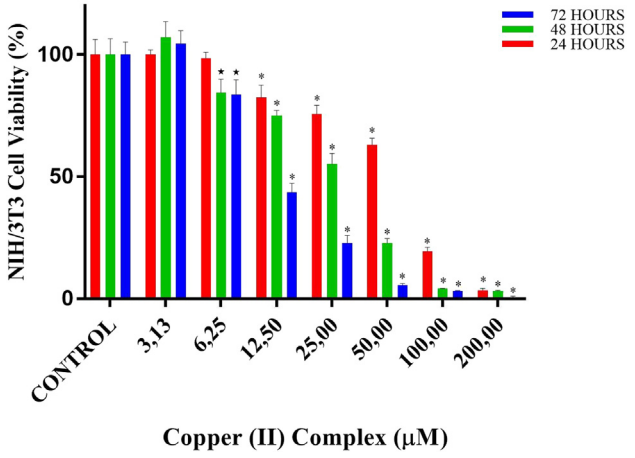

Fig. 8 Cell viability percentages of NIH/3T3 cells vs different doses of copper(II) complex according to MTT assay results. * designates significant difference of $p < 0.001$ when compared to control group.

despite a downward trend (89.5%, $p > 0.05$) in cell viability. However, at the doses of 50, 100 and 200 μM, cell viabilities decreased to 82.9 ($p < 0.05$), 82.0 ($p < 0.05$) and 76.1% ($p < 0.01$), respectively. In the 72-hour treatment, similarly, at the doses of 25, no significant difference was detected when compared to control, despite a downward trend (86.9%, $p > 0.05$) in cell viability. However, at the doses of 50, 100 and 200 μM, cell viabilities decreased to 81.7 ($p < 0.05$), 80.7 ($p < 0.05$) and 65.1% ($p < 0.01$), respectively.

According to MTT results of BIPY, in the 24-hour treatment, at all the doses, no significant difference in cell viability was detected when compared to control ($p > 0.05$). In the 48-hour treatment, at the dose of 25, no significant difference in cell viability was detected when compared to control ($p > 0.05$). However, at the doses of 50, 100 and 200 μM, cell viabilities decreased to 74.0, 70.0 and 62.6% (all $p < 0.001$), respectively. In the 72-hour treatment, at the dose of 25, no significant difference in cell viability was detected when compared to control ($p > 0.05$). However, at the doses of 50, 100 and

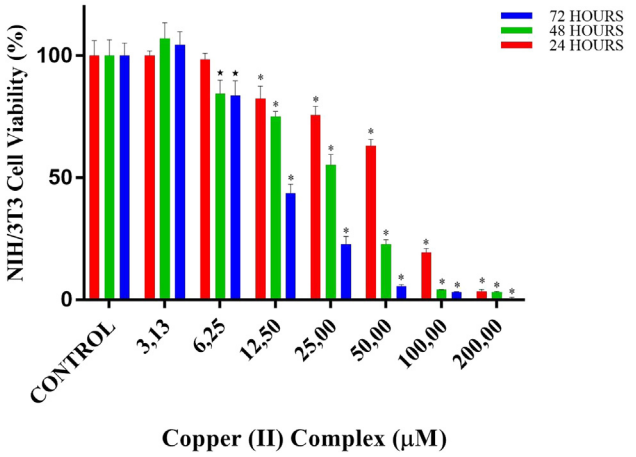

Fig. 9 Cell viability percentages of SPC212 cells vs different doses of copper(II) complex according to MTT assay results. • and * designates significant difference of $p < 0.05$ and $p < 0.001$ when compared to control group.

Table 3 Viability percentages of NIH/3T3 cells after 24-, 48- and 72-hour copper(II) complex treatment.

copper(II) complex doses (μM)	MTT SPC212 Cell viability (%) (mean ± SD)		
	24 h	48 h	72 h
Untreated	100.0 ± 6.3	100.0 ± 6.6	100.0 ± 5.1
3.13	100.1 ± 1.9	107.1 ± 6.4	104.5 ± 5.4
6.25	98.5 ± 2.5	84.5 ± 5.6★	83.6 ± 6.1★
12.5	82.4 ± 5.1*	75.1 ± 2.0*	43.6 ± 3.7*
25.0	75.7 ± 3.5*	55.3 ± 4.3*	22.9 ± 3.1*
50.0	63.0 ± 2.7*	22.8 ± 1.9*	5.6 ± 0.6*
100.0	19.3 ± 1.7*	4.2 ± 0.1*	3.2 ± 3.1*
200.0	3.5 ± 0.7*	3.2 ± 0.3*	0.7 ± 0.4*

★ and * designates significant difference of $p < 0.01$ and $p < 0.001$ when compared to control group.

200 μM, cell viabilities decreased to 53.1, 43.2, and 49.4% (all $p < 0.001$), respectively.

According to MTT results of copper (II) complex for NIH/3T3 cells, in the 24-hour treatment, cell viabilities at doses of 3.13 and 6.25 μM were close to that in control. The first significant decrease in viability was detected at 12.5 μM of copper (II) complex ($p < 0.001$ vs control), where the viability was 82.4%. This decrease in viability at the doses of 25, 50 and 100 μM became 75.7, 63.0 and 19.3%, respectively (both $p < 0.001$ vs control). Almost no cell viability was observed at 200 μM. In the 48-hour treatment, cell viabilities at the doses of 3.13 μM was close to that in control. The first significant reduction was observed at 6.25 μM of copper(II) complex, where the viability decreased to 84.5% ($p < 0.01$vs control). At the dose of 12.5, 25 and 50 μM, viability decreased to 75.1, 55.3 and 22.8% ($p < 0.001$vs control). At the doses of 100 and 200, viability was <5%. In the 72-hour treatment, at the dose of 6.25, cellular viability decreased almost by %20. At the dose of 12.5, cellular viability decreased more than %50 ($p < 0.001$ vs control). At the dose of 25.0, the viability was 22.8%. At the higher doses, the viability was lower than % 10 (Table 3 and Fig. 8).

Table 4 Viability percentages of SPC212 cells after 24-, 48- and 72-hour copper(II) complex treatment.

copper(II) complex doses (μM)	MTT SPC212 Cell viability (%) (mean ± SD)		
	24 h	48 h	72 h
Untreated	100.0 ± 4.4	100.0 ± 8.6	100.0 ± 5.3
3.13	100.2 ± 6.8	95.0 ± 8.7	90.6 ± 8.2
6.25	99.9 ± 4.3	94.2 ± 10.5	90.5 ± 3.6•
12.5	87.1 ± 7.1•	70.8 ± 12.5*	66.7 ± 5.5*
25.0	62.5 ± 12.2*	58.8 ± 5.2*	45.6 ± 4.6*
50.0	46.5 ± 7.7*	36.7 ± 3.3*	18.6 ± 3.4*
100.0	34.7 ± 4.2*	6.1 ± 1.8*	0.1 ± 1.1*
200.0	0.1 ± 2.3*	0.0 ± 0.4*	0.0 ± 0.1*

• and * designates significant difference of $p < 0.05$ and $p < 0.001$ when compared to control group.

Table 5 Viability percentages of DU145 cells after 24-, 48- and 72-hour copper(II) complex treatment.

copper(II) complex doses (μM)	MTT DU145 Cell viability (%) (mean ± SD)		
	24 h	48 h	72 h
Untreated	100.0 ± 7.9	100.0 ± 7.3	100.0 ± 13.7
3.13	100.7 ± 3.9	96.2 ± 0.7	73.3 ± 3.3•
6.25	103.8 ± 5.0	89.0 ± 10.9	58.2 ± 9.5*
12.5	89.6 ± 4.4	72.0 ± 6.6*	44.7 ± 11.2*
25.0	70.0 ± 3.8*	40.1 ± 3.6*	18.3 ± 6.7*
50.0	28.6 ± 2.1*	5.1 ± 2.3*	0.2 ± 0.7*
100.0	13.5 ± 5.1*	2.2 ± 1.8*	0.4 ± 1.0*
200.0	1.6 ± 1.5*	4.4 ± 5.9*	± 0.5*

• and * designates significant difference of $p < 0.05$ and $p < 0.001$ when compared to control group.

According to MTT results of copper (II) complex for SPC212 cells, in the 24-hour treatment, cell viabilities at doses of 3.13 and 6.25 μM were close to that in control. The first significant decrease in viability was detected at 12.5 μM of copper (II) complex ($p < 0.05$vs control), where the viability was 87.1%. This decrease in viability at the doses of 25, 50 and 100 μM became 62.5, 46.5 and 34.7%, respectively (both $p < 0.001$ vs control). No cell viability was observed at 200 μM. In the 48-hour treatment, cell viabilities at the doses of 3.13 and 6.25 μM were close to that in control. The first significant reduction was observed at 12.5 μM of copper(II) complex, where the viability decreased to 70.8% ($p < 0.001$ vs control). At the dose of 25 and 50 μM, viability decreased to 58.8 and 36.7% ($p < 0.001$ vs control). At the dose of 100 μM, viability was below 10%. No cell viability was observed at 200 μM. In the 72-hour treatment, although the viability percentages at 3.13 and 6.25 μM were similar, only the latter showed a significant reduction ($p < 0.05$), resulting from the intragroup variation. At the doses of 12.5, 25 and 50 μM, the cell viabilities were 66.7, 45.6 and 18.6%, respectively (both $p < 0.001$ vs control). At the doses of 100 and 200 μM, no cell viability was detected (Table 4 and Fig. 9).

According to MTT results of copper(II) complex for DU145 cells, in the 24-h treatment, cell viabilities at doses of 3.13 and 6.25 μM were close to that in control. Although the first decrease in viability was observed at 12.5 μM of copper (II) complex, it was not statistically significant. The first significant reduction was observed at 25 μM of copper(II) complex, where the viability decreased to 70% ($p < 0.001$ vs control). This decrease in viability at the doses of 50 and 100 μM became 28.6 and 13.5%, respectively (both $p < 0.001$vs control). Almost no cell viability was observed at 200 μM, which was the highest dose of copper(II) complex applied. In the 48-hour treatment, cell viability at the dose of 3.13 μM was close to that in control. Although the first decrease in viability was observed at 6.25 μM of copper(II) complex, it was not statistically significant. The first significant reduction was observed at 12.5 μM of copper(II) complex, where the viability decreased to 72% ($p < 0.001$ vs control). At the dose of 25 μM, viability decreased to 40% ($p < 0.001$ vs control). At the doses of 50, 100 and 200 μM, viability was below 10%. In the 72-hour treatment, a statistically significant decrease in cell viability was observed even at the lowest dose of copper(II) complex used ($p < 0.001$vs control), the viability of which was 73.3%. At the doses of 6.25 and 12.5 μM cell viabilities were 58.2 and 44.7%, respectively (both $p < 0.001$ vs control). At a dose of 25 μM, the viability decreased further to 18.3%, and no cell viability was observed at the highest 3 doses (Table 5 and Fig. 10).

IC_{50} values of copper(II) complex against NIH/3T3 normal fibroblast cells were 64.9 μM for 24 h-, 29.1 μM for 48 h- and 11.5 μM for 72h-long treatments. On the other hand, IC_{50} values of copper(II) complex at 24, 48 and 72 h-long treatments against SPC212 cells were 44.5, 35.0 and 22.4 μM, while against DU145 cells were 37.0, 21.1 and 10.0 μM, respectively. Subsequent experiments were continued with DU145 cells because the complex inhibited these cells more efficiently. The copper(II) complex doses to be used in the subsequent experiments were ascertained according to the results of 24-hour MTT of DU145 cells. In this respect, IC_{50} (37 μM), the doses just lower (25 μM) and higher than IC_{50} (50 μM) were selected from the MTT results for subsequent analyses. In biochemical analysis, inverted microscope analysis and H-E staining, all these three doses were used, while in DAPI and May-Grunwald-Giemsa analysis only doses of 37 and 50 μM were

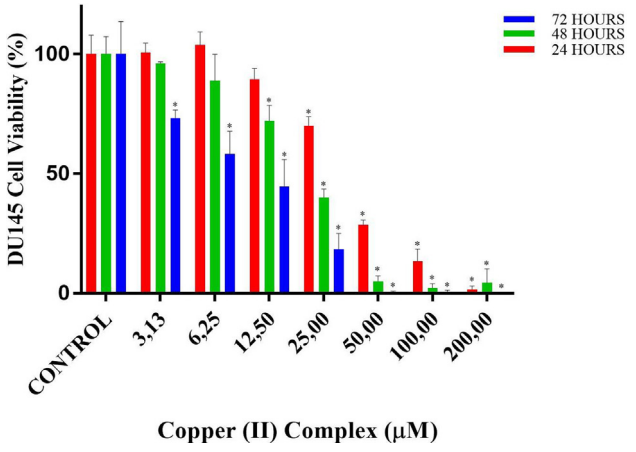

Fig. 10 Cell viability percentages of DU145 cells vs different doses of copper(II) complex according to MTT assay results. • and * designate significant difference of $p < 0.05$ and $p < 0.001$ when compared to control.

used. On the other hand, in immunocytochemistry, the lower doses, 25 and 37 μM were used to observe the protein expressions before cells undergo death.

3.4. Effect of copper(II) complex on oxidative status

In TOS analysis, 25 and 37 μM of copper(II) complex increased TOS levels more than 2 folds (both $p > 0.05$ vs control). At the dose of 50 μM, this increase was 3.5 fold (both $p > 0.001$ vs control). In TAS analysis, the TAS levels of the treated groups decreased in a dose-dependent manner. The lowest TAS level was observed at the dose of 50 μM, which was less than half of the control level ($p < 0.001$). Finally, according to the OSI results, At the doses of 25 and 37 μM, there was an increase around 3 folds (both $p < 0.01$). However, at the highest dose, OSI level was almost 9.5 times higher than that of the control ($p > 0.001$) (see Fig. 11).

3.5. Effect of copper(II) complex on ER stress

According to the Western blot results, at 25 μM of copper(II) complex the expression of GRP78 increased more than 8 folds ($p < 0.001$ vs control). At 37 μM, this increase persisted. At the highest treated dose, 50 μM, the expression of GRP78 was decreased by half. However, it was still significantly higher than control levels (almost 4.5 folds, $p > 0.001$) (see Fig. 12).

3.6. Effects of copper(II) complex on cell morphology

As to the morphological observations (Figs. 13 and 14), there was mild to moderate degeneration on the cells at the dose of 25 μM copper(II) complex. However, the cells almost lost their characteristic morphology and became rounded and shrunken at the dose of 37 μM copper(II) complex. The degenerative changes at 37 μM persisted and even became more serious at the dose of 50 μM copper(II) complex; besides, the number of cells reduced considerably.

3.7. Immunocytochemistry results

Bax staining is depicted in Fig. 15, including untreated, 37 and 50 μm of copper(II) complex-treated cells. In Bax staining, untreated cells were barely stained, while copper(II) complex-treated cells were well-stained. Furthermore, the intensity of staining increased more at the highest-applied dose, 50 μm of copper(II) complex.

PCNA staining is depicted in Fig. 16, including untreated, 37 and 50 μm of copper(II) complex-treated cells. In PCNA staining, untreated cells are well-stained. In 37 μM of copper (II) complex-treated cells, the number of stained cells decreased, that is, while some cells were immune-positive, some were not. In 50 μM of copper(II) complex-treated cells, PCNA staining was almost negative. No apparent staining was observable.

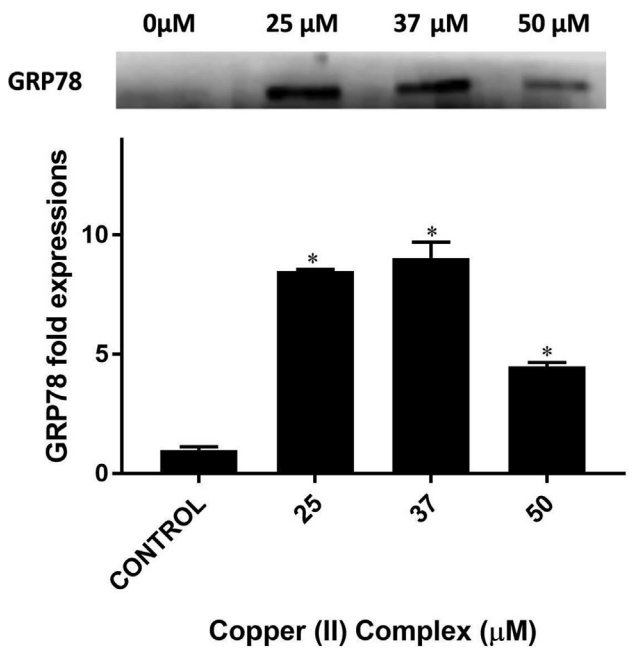

Fig. 12 Western blot bands and respective fold expressions of GRP78 protein in Copper (II) complex-treated DU-145 cells. * $p < 0.001$ when compared to the control group.

4. Discussion

In the present study, a novel pyridyl-fluorobenzimidazole-derived copper complex was synthesized, its crystal structure was disclosed and its apoptotic, morphologic, proliferative effects on DU145 prostate cancer cells were scrutinized. We

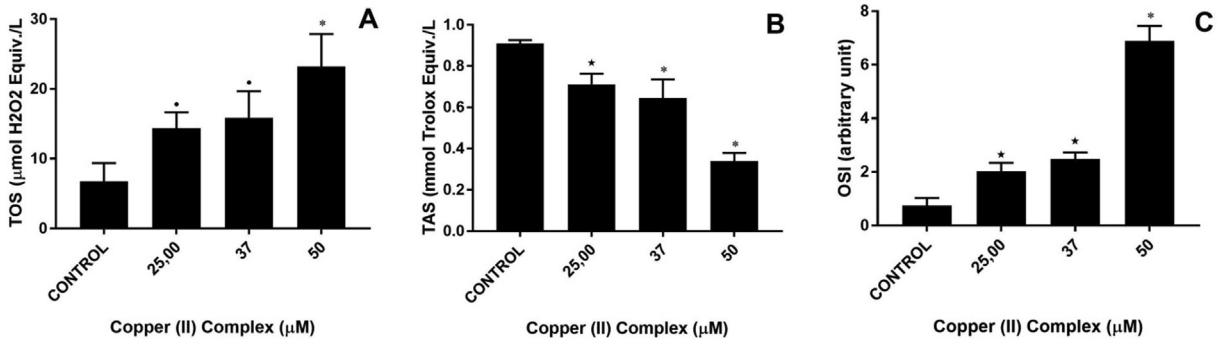

Fig. 11 Total oxidant status (TOS), total antioxidant status (TAS) and oxidative stress index (OSI) of Copper (II) complex-treated DU-145 cells. A: TOS, B: TAS and C: OSI levels. •$p < 0.05$, ★$p < 0.01$ and *$p < 0.001$ when compared to the control group.

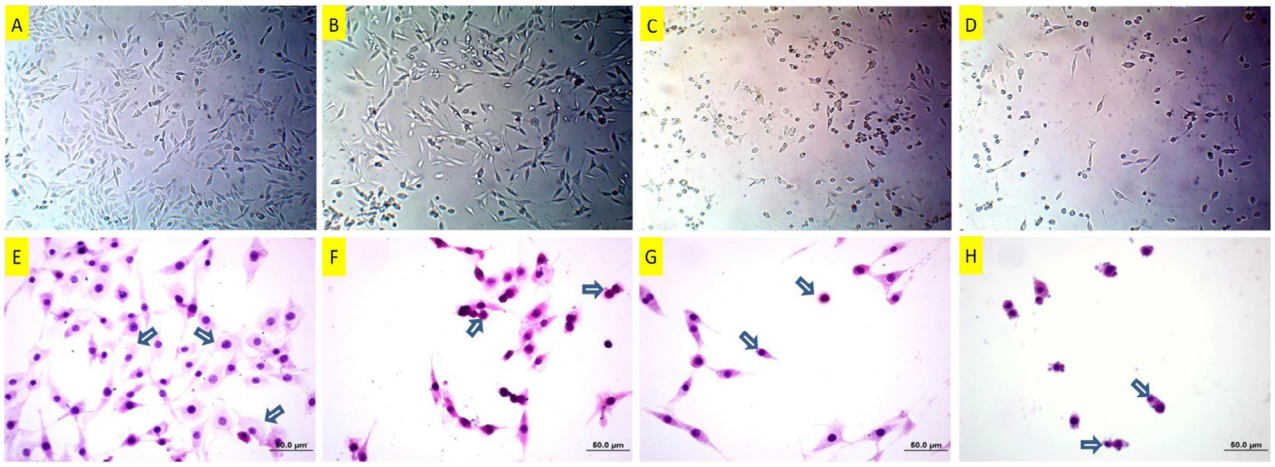

Fig. 13 Inverted microscope images (**A-D**) of DU145 cells following copper(II) complex treatment. **A**: Untreated cells, **B**: 25 μM, **C**: 37 μM and **D**:50 μM, copper(II) complex-treated cells for 24 h. While there are mild degenerations in the low dose –treated cells in A, particularly the cells in C and D are damaged more. Hematoxylin-eosin staining (**E-H**) of DU145 cells following copper(II) complex treatment. **E**: Untreated DU145 cells. *Arrows*: Normal cells with gross cytoplasm and standard nuclei. **F**: 25 μM of copper(II) complex-treated DU145 cells. *Arrows*: Condensed cell and cell with membrane blebbing. **G**: 37 μM of copper(II) complex-treated DU145 cells. *Arrows*: Condensed and shrunken cells. **H**: 50 μM of copper(II) complex-treated DU145 cells. *Arrows*: Condensed and shrunken cells.

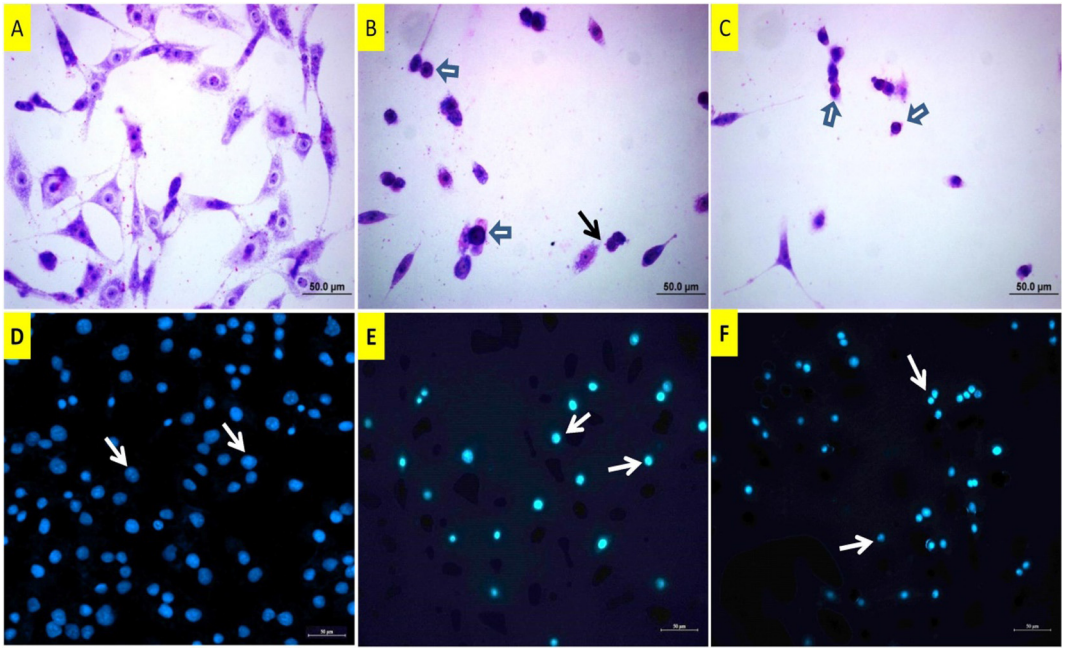

Fig. 14 May Grunwald images (A-C) of DU145 cells following copper(II) complex treatment. **A**: Untreated cells, **B**: 37 μM and **C**: 50 μM of copper(II) complex-treated cells for 24 h. *White arrow*: Shrunken and rounded cells with condensed nuclei, *black arrow:* Membrane blebbing. DAPI staining (**D-F**) of DU145 cells. **D**: Untreated cells, a*rrows:* normal size nuclei. **E:** 37 μM of copper(II) complex-treated cells, *arrows*: Pyknotic nuclei. **F:** 50 μM of copper(II) complex-treated cells, *arrows*: Pyknotic nuclei.

searched not only the antiproliferative effect of the newly synthesized copper(II) complex on NIH/3T3, DU145 and SPC212 cells but also the effects of the chemicals from which it was synthesized (CF, CU, BIPY) on DU145 cells. Based on the MTT results, we clearly state that copper(II) complex has stronger anti-cancer activity on DU145 cells than its chemical components, demonstrating its potency to inhibit cancer cells and to be focused on.

Briefly, IC_{50} concentrations of copper(II) complex against DU145 cells were found as 37.0 μM for 24 h, 21.1 μM for 48 h and 10.0 μM for 72 h. On the other hand, IC_{50} of all its chemical components could not be calculated because the maximum dose we used in the experiment (200 μM) did not inhibit the 50% of the cells and nor did show a sufficient inhibitory effect. For the calculable ones, all IC_{50} values were greater than 100 μM. In this context, copper (II) complex proved to

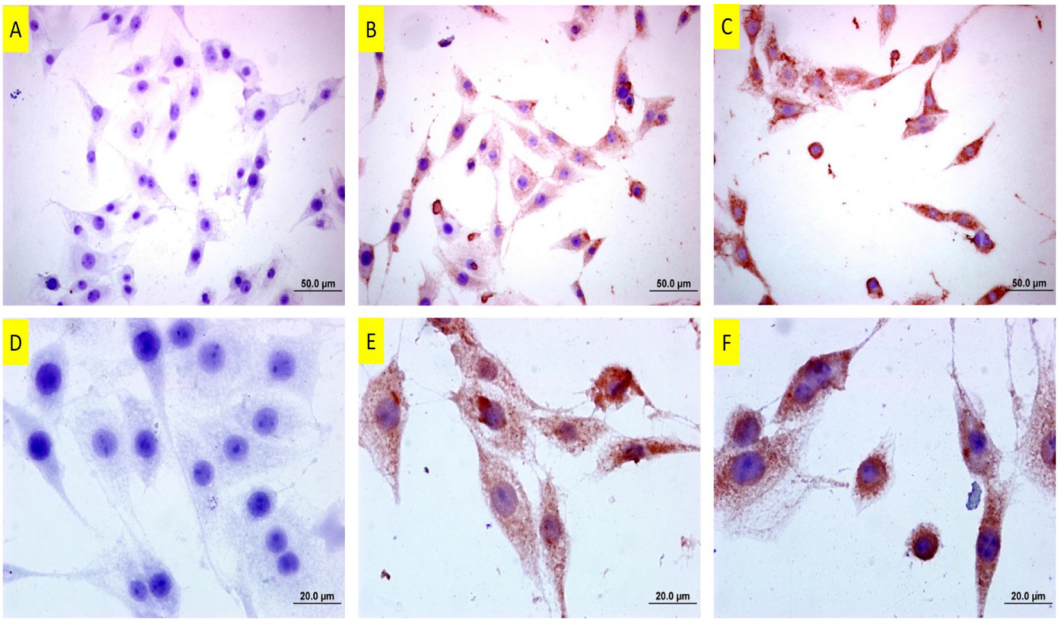

Fig. 15 Bax staining of DU145 cells following copper(II) complex treatment. **A**: Untreated cells. Note of almost no positive staining **B**: 25 µM and **C**: 37 µM of copper(II) complex-treated cells for 24 h. Note that the cells are immune-positive and the intensity of staining is even more at the higher dose. The bars in A, B and C indicate 50 µm and bars in D, E and F indicate 20 µm.

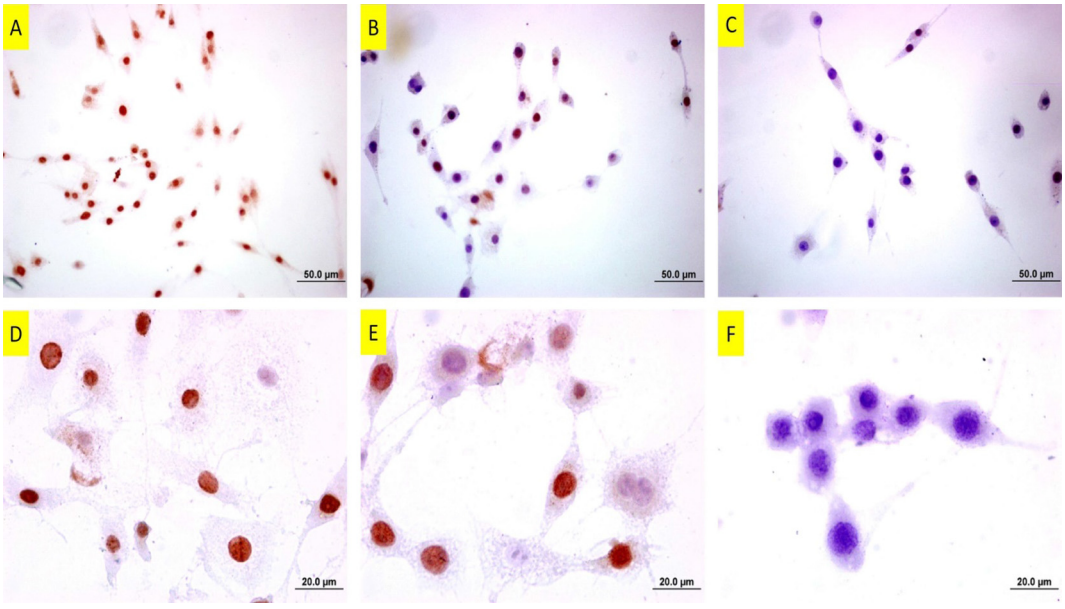

Fig. 16 PCNA staining of DU145 cells following copper(II) complex treatment. A: Untreated cells. Note of the number of intensely-stained cells B: 25 µM and C: 37 µM of copper(II) complex-treated cells for 24 h. Note that the stained cells decreased at the dose of 25 µM, and there are barely stained cells at the dose of 37 µM. The bars in A, B and C indicate 50 µm and bars in D, E and F indicate 20 µm.

be superior to its separate chemical components in the present study. For NIH/3T3 cells IC_{50} concentrations were 64.9 µM for 24 h, 29.1 µM for 48 h and 11.5 µM for 72 h. As such, we can posit that DU145 cells are more sensitive to the complex than NIH/3T3 normal fibroblast cells. On the other hand, IC_{50} concentrations of the complex for SPC212 cells were 44.5 µM for 24 h, 35.0 µM for 48 h and 22.4 µM for 72 h, referring that SPC212 cells were more resistant to the complex than both DU145 and NIH/3T3 cells. In literature, Zhao et al. tested novel benzimidazole copper complexes against SMMC7721, BGC823, HCT116, HT29 cell lines and found IC_{50} concentrations lower than 10 µM in all cell lines for 24 h (Ja et al., 2017). In the study of Qui et al., IC_{50}s of the 48-hour-treated copper complexes were found 8.58 and 8.39 µM for A549, 16.33 and 11.49 µM for PC-3 prostate cancer cells and 11.67 and 7.88 µM for HeLa cells (Qi et al., 2018).

In our study, we found IC_{50} of copper(II) complex for 48 h as 21.1 μM against DU145 cells and 35.0 μM for SPC212 cells. Our relatively higher IC_{50}s can be stemmed from cell line type or the activity strength of chemicals due to different moieties bound to them. Even the IC_{50} doses of the cells derived from same tissue type can change. To exemplify, in the study of Wang et al., reported IC_{50} values for 10 prostate cancer cell lines differed considerably (Wang et al., 2011). It is also noteworthy that IC_{50} values against DU145 cells in the study were the highest.

Apoptosis is programmed cell death with distinctive morphological and protein-expression profile characteristics, stemming from several causes, including, excessive oxidative burden, apoptosis-inducing chemicals. Morphological changes include membrane blebbing, nuclear condensation, cellular shrinkage, formation of apoptotic bodies, nuclear and DNA fragmentations (Martelli et al., 2001). Regarding protein profiles, the proteins known as pro-apoptotic, such as Bax, Bad and Bid, etc. increase, while the proteins known as anti-apoptotic, such as Bcl-2, etc. decrease. In our study, we examined apoptosis at morphological and protein-expression levels by immunocytochemistry for Bax.

In the microscopic examinations and stainings, we observed several apoptotic hallmarks, such as nuclear condensation, cellular shrinkage and membrane blebbings. We approved these morphological changes by observing increased Bax protein dose-dependently in immunocytochemistry. In this respect, there are numerous studies in the literature regarding apoptosis. Newly synthesized benzimidazole copper complexes induced apoptosis in HCT116 cells (Ja et al., 2017). Qui et al. synthesized two new Cu (II) complexes based on 5-methyl-2-(2′-pyridyl) benzimidazole and reported their apoptotic effects on HeLa cells via mitochondrial dysfunction pathway induced by ROS (Qi et al., 2018). These complexes induced nuclear condensation and chromatin alteration and upregulated proapoptotic proteins Bad and Bax in HeLa cells. Besides, benzimidazole-based copper complexes of Hu et al. was purported to induce apoptosis in HCT116 cells via generating ROS and inflicting damage on DNA and mitochondrion (Hu et al., 2017).

Main action mechanism of copper complexes is well-known to be through DNA binding and cleavage, in which DNA is degraded by Fenton-type reaction and ROS reveals when reducing agents are available (Iakovidis et al., 2011; Wang et al., 2010). Apart from their direct cleavage of DNA and RNA, they also engender oxidative damage by displacement of other metal ions, lipid peroxidization and ROS induction. (Halliwell and Gutteridge, 1990; Marzano et al., 2009). In our study, the newly synthesized copper (II) complex increased TOS and decreased TAS levels, thereby raising the OSI levels. OSI is a reliable indicator indicating the oxidant-antioxidant balance by evaluating total antioxidant and oxidant status. In the present study, higher OSI levels in copper-treated groups refer to the oxidative stress-inducing effect of copper in cancer cells. In one study, Isatin-Schiff base copper(II) complexes were reported to increase ROS and oxidative stress in SH-SY5Y neuroblastoma cells (Filomeni et al., 2007). In another study, copper and iron complexes with 8-hydroxyquinoline derivatives caused oxidative stress and led to cell death in Hela cervical cancer cells (Barilli et al., 2014). Besides, copper-thiosemicarbazone complexes were shown to activate oxygen species and inhibit the growth of Ehrlich ascites tumor cells (Byrnes et al., 1990).

ER stress is the unfolded protein response stemming from the accumulation of improperly folded or unfolded proteins in ER lumen. When the number of unfolded proteins rises, to assist proper protein folding, an increase in the amount of GRP78, an ER stress marker, is observed. Bortolozzi et al. treated leukemia cells with a phosphine copper(I) complex and this complex augmented the levels of ubiquitinated proteins and ER stress markers, including GRP78, CHOP ve XBP1(Bortolozzi et al., 2014). Gandin et al. posited that a novel copper complex led to paraptosis in colon cancer cells by initiating ER stress (Gandin et al., 2012). What's more, a thioxotriazole copper(II) complex was also shown to induce ER stress in several human cancer cell lines (Tardito et al., 2009). In very recent study, also, mixed copper(II)-phenanthroline complexes were exhibited to trigger ER stress in ovarian cancer cells (Moran et al., 2019). In our study we also showed that our copper complex induced ER stress significantly in all the treated doses. Our complex might be activated over ER stress pathway.

In summary, we described the synthesis and characterization of a novel mononuclear copper (II) complex. The complex showed anti-proliferative and apoptotic effects on the cancer cells, and its IC50 values for DU145 prostate cancer and SPC212 mesothelioma cells were shared with literature. Metal complexes, especially copper-containing ones are auspicious for the discovery of new cancer drugs with low IC_{50} and fewer side effects. Given that there are many possible combinations to do and produce a versatile complex, future studies should be more focused on this area.

Acknowledgements

We thank the Medicinal Plants and Medicine Research Centre of Anadolu University, Eskişehir, Turkey for the use of X-ray Diffractometer, Eskisehir Technical University, Chemistry Department, Eskişehir, Turkey for the other spectroscopic measurements and Eskisehir Osmangazi University, Turkey Central Research Laboratory Application and Research Center for the usage of fluorescent microscope.

Appendix A. Supplementary material

CCDC 1893373 contains the supplementary crystallographic data for copper(II) complex. Supplementary data to this article can be found online at https://doi.org/10.1016/j.arabjc.2019.08.002.

References

Apelgot, S., Coppey, J., Fromentin, A., Guille, E., Poupon, M.F., Roussel, A., 1986. Altered distribution of copper (64Cu) in tumor-bearing mice and rats. Anticancer Res. 6 (2), 159–164.

Balakrishna, M.S., Suresh, D., Rai, A., Mague, J.T., Panda, D., 2010. Dinuclear copper(I) complexes containing cyclodiphosphazane derivatives and pyridyl ligands: synthesis, structural studies, and antiproliferative activity toward human cervical and breast cancer cells. Inorg. Chem. 49 (19), 8790–8801.

Barilli, A., Atzeri, C., Bassanetti, I., Ingoglia, F., Dall'Asta, V., Bussolati, O., et al, 2014. Oxidative stress induced by copper and

iron complexes with 8-hydroxyquinoline derivatives causes paraptotic death of HeLa cancer cells. Mol. Pharm. 11 (4), 1151–1163.
Bortolozzi, R., Viola, G., Porcu, E., Consolaro, F., Marzano, C., Pellei, M., et al, 2014. A novel copper(I) complex induces ER-stress-mediated apoptosis and sensitizes B-acute lymphoblastic leukemia cells to chemotherapeutic agents. Oncotarget. 5 (15), 5978–5991.
Boyle, K.M., Barton, J.K., 2018. A family of rhodium complexes with selective toxicity toward mismatch repair-deficient cancers. J. Am. Chem. Soc. 140 (16), 5612–5624.
Burke, C.S., Byrne, A., Keyes, T.E., 2018. Targeting photoinduced DNA destruction by Ru(II) tetraazaphenanthrene in live cells by signal peptide. J. Am. Chem. Soc. 140 (22), 6945–6955.
Byrnes, R.W., Mohan, M., Antholine, W.E., Xu, R.X., Petering, D.H., 1990. Oxidative stress induced by a copper-thiosemicarbazone complex. Biochemistry 29 (30), 7046–7053.
Chan, J.K., 2014. The wonderful colors of the hematoxylin-eosin stain in diagnostic surgical pathology. Int. J. Surg. Pathol. 22 (1), 12–32.
Clark, G., 1981. In: Clark, G. (Ed.), Staining Procedures. 4th Edition. Williams & Wilkins, Baltimore, London.
Dolomanov, O.V., Bourhis, L.J., Gildea, R.J., Howard, J.A.K., Puschmann, H., 2009. OLEX2: a complete structure solution, refinement and analysis program. J. Appl. Crystallogr. 42 (2), 339–341.
dos Santos Silva, T.D., Bomfim, L.M., da Cruz Rodrigues, A.C.B., Dias, R.B., Sales, C.B.S., Rocha, C.A.G., et al, 2017. Anti-liver cancer activity in vitro and in vivo induced by 2-pyridyl 2,3-thiazole derivatives. Toxicol. Appl. Pharmacol. 329, 212–223.
Fan, C., Su, H., Zhao, J., Zhao, B., Zhang, S., Miao, J., 2010. A novel copper complex of salicylaldehyde pyrazole hydrazone induces apoptosis through up-regulating integrin β4 in H322 lung carcinoma cells. Eur. J. Med. Chem. 45 (4), 1438–1446.
Filomeni, G., Cerchiaro, G., Da Costa Ferreira, A.M., De Martino, A., Pedersen, J.Z., Rotilio, G., et al, 2007. Pro-apoptotic activity of novel Isatin-Schiff Base copper(II) complexes depends on oxidative stress induction and organelle-selective. Damage. 282 (16), 12010–12021.
Florea, A.-M., Büsselberg, D., 2011. Cisplatin as an anti-tumor drug: cellular mechanisms of activity. Drug Resistance Induced Side Effects. 3 (1), 1351–1371.
Gandin, V., Pellei, M., Tisato, F., Porchia, M., Santini, C., Marzano, C., 2012. A novel copper complex induces paraptosis in colon cancer cells via the activation of ER stress signalling. J. Cell Mol. Med. 16 (1), 142–151.
Gellis, A., Kovacic, H., Boufatah, N., Vanelle, P., 2008. Synthesis and cytotoxicity evaluation of some benzimidazole-4,7-diones as bioreductive anticancer agents. Eur. J. Med. Chem. 43 (9), 1858–1864.
Halliwell, B., Gutteridge, J.M., 1990. Role of free radicals and catalytic metal ions in human disease: an overview. Methods Enzymol. 186, 1–85.
Hranjec, M., Starčević, K., Pavelić, S.K., Lučin, P., Pavelić, K., Karminski, Zamola G., 2011. Synthesis, spectroscopic characterization and antiproliferative evaluation in vitro of novel Schiff bases related to benzimidazoles. Eur. J. Med. Chem. 46 (6), 2274–2279.
Hu, J., Liao, C., Guo, Y., Yang, F., Sang, W., Zhao, Ja., 2017. Copper (II) complexes inducing apoptosis in cancer cells, and demonstrating DNA and HSA interactions. Polyhedron 132, 28–38.
Iakovidis, I., Delimaris, I., Piperakis, S.M., 2011. Copper and Its complexes in medicine: A biochemical approach. J. Mol. Biol. Int. 2011.
Ja, Zhao, Zhi, S., Yu, H., Mao, R., Hu, J., Song, W., et al, 2017. Mitochondrial and nuclear DNA dual damage induced by 2-(2′-quinolyl)benzimidazole copper complexes with potential anticancer activity. RSC Adv. 7 (81), 51162–51174.
Kang, T.-S., Wang, W., Zhong, H.-J., Dong, Z.-Z., Huang, Q., Mok, S.W.F., et al, 2017. An anti-prostate cancer benzofuran-conjugated iridium(III) complex as a dual inhibitor of STAT3 and NF-κB. Cancer Lett. 396, 76–84.
Khalil, N.A., Kamal, A.M., Emam, S.H., 2015. Design, synthesis, and antitumor activity of novel 5-pyridyl-1,3,4-oxadiazole derivatives against the breast cancer cell line MCF-7. Biol. Pharm. Bull. 38 (5), 763–773.
Kumar, M., Mogha, N.K., Kumar, G., Hussain, F., Masram, D.T., 2019. Biological evaluation of copper(II) complex with nalidixic acid and 2,2′-bipyridine (bpy). Inorganica Chim. Acta 490, 144–154.
Liu, Y.-X., Mo, H.-W., Lv, Z.-Y., Shen, F., Zhang, C.-L., Qi, Y.-Y., et al, 2018. DNA binding, crystal structure, molecular docking studies and anticancer activity evaluation of a copper(II) complex. Transition Metal Chem. 43 (3), 259–271.
Liu, L.-J., Wang, W., Huang, S.-Y., Hong, Y., Li, G., Lin, S., et al, 2017. Inhibition of the Ras/Raf interaction and repression of renal cancer xenografts in vivo by an enantiomeric iridium(iii) metal-based compound. Chem. Sci. 8 (7), 4756–4763.
Lygin, A.V., de Meijere, A., 2009. Synthesis of 1-substituted benzimidazoles from o-bromophenyl isocyanide andamines. Eur. J. Organic Chem. 2009 (30), 5138–5141.
Macrae, C.F., Bruno, I.J., Chisholm, J.A., Edgington, P.R., McCabe, P., Pidcock, E., et al, 2008. Mercury CSD 2.0 - new features for the visualization and investigation of crystal structures. J. Appl. Crystallogr. 41 (2), 466–470.
Martelli, A.M., Zweyer, M., Ochs, R.L., Tazzari, P.L., Tabellini, G., Narducci, P., et al, 2001. Nuclear apoptotic changes: an overview. J. Cell. Biochem. 82 (4), 634–646.
Marzano, C., Pellei, M., Tisato, F., Santini, C., 2009. Copper complexes as anticancer agents. Anti-Cancer Agents Med. Chem. 9 (2), 185–211.
Moran, L., Pivetta, T., Masuri, S., Vasickova, K., Walter, F., Prehn, J., et al, 2019. Mixed copper(ii)-phenanthroline complexes induce cell death of ovarian cancer cells by evoking the unfolded protein response. Metallomics : Integrated Biometal Sci.
Qi, Y.-Y., Gan, Q., Liu, Y.-X., Xiong, Y.-H., Mao, Z.-W., Le, X.-Y., 2018. Two new Cu(II) dipeptide complexes based on 5-methyl-2-(2′-pyridyl)benzimidazole as potential antimicrobial and anticancer drugs: Special exploration of their possible anticancer mechanism. Eur. J. Med. Chem. 154, 220–232.
Refaat, H.M., 2010. Synthesis and anticancer activity of some novel 2-substituted benzimidazole derivatives. Eur. J. Med. Chem. 45 (7), 2949–2956.
Salahuddin, Shaharyar, M., Mazumder, A., 2017. Benzimidazoles: A biologically active compounds. Arabian J. Chem. 10, S157–S173.
Santini, C., Pellei, M., Gandin, V., Porchia, M., Tisato, F., Marzano, C., 2014. Advances in copper complexes as anticancer agents. Chem. Rev. 114 (1), 815–862.
Sheldrick, G., 2008. A short history of SHELX. Acta Crystall. Section A. 64 (1), 112–122.
Sheldrick, G., 2015. Crystal structure refinement with SHELXL. Acta Crystall. Section C. 71 (1), 3–8.
Tardito, S., Isella, C., Medico, E., Marchio, L., Bevilacqua, E., Hatzoglou, M., et al, 2009. The thioxotriazole copper(II) complex A0 induces endoplasmic reticulum stress and paraptotic death in human cancer cells. J. Biol. Chem. 284 (36), 24306–24319.
Thimmegowda, N.R., Nanjunda Swamy, S., Kumar, C.S., Kumar, Y. C., Chandrappa, S., Yip, G.W., et al, 2008. Synthesis, characterization and evaluation of benzimidazole derivative and its precursors as inhibitors of MDA-MB-231 human breast cancer cell proliferation. Bioorg. Med. Chem. Lett. 18 (1), 432–435.
Unver, H., 2018. Crystal structure of an alkoxide bridged dinuclear copper(II) complex: mild and selective oxidation of primary and secondary alcohols in water. Transit. Metal Chem. 43 (7), 641–646.
Wang, W., Lee, Y.A., Kim, G., Kim, S.K., Lee, G.Y., Kim, J., et al, 2015. Oxidative DNA cleavage by Cu(II) complexes: Effect of periphery substituent groups. J. Inorg. Biochem. 153, 143–149.

Wang, X., Ma, D., Olson, W.C., Heston, W.D., 2011. In vitro and in vivo responses of advanced prostate tumors to PSMA ADC, an auristatin-conjugated antibody to prostate-specific membrane antigen. Mol. Cancer Ther. 10 (9), 1728–1739.

Wang, W., Vellaisamy, K., Li, G., Wu, C., Ko, C.N., Leung, C.H., et al, 2017. Development of a long-lived luminescence probe for visualizing beta-galactosidase in ovarian carcinoma cells. Anal. Chem. 89 (21), 11679–11684.

Wang, Y., Zhang, X., Zhang, Q., Yang, Z., 2010. Oxidative damage to DNA by 1,10-phenanthroline/L: -threonine copper (II) complexes with chlorogenic acid. Biometals : Int. J. Role Metal Ions Biol., Biochem., Med. 23 (2), 265–273.

Yang, G.J., Wang, W., Mok, S.W.F., Wu, C., Law, B.Y.K., Miao, X. M., et al, 2018. Selective inhibition of lysine-specific demethylase 5A (KDM5A) using a rhodium(III) complex for triple-negative breast cancer therapy. Angew. Chem. (International ed in English) 57 (40), 13091–13095.